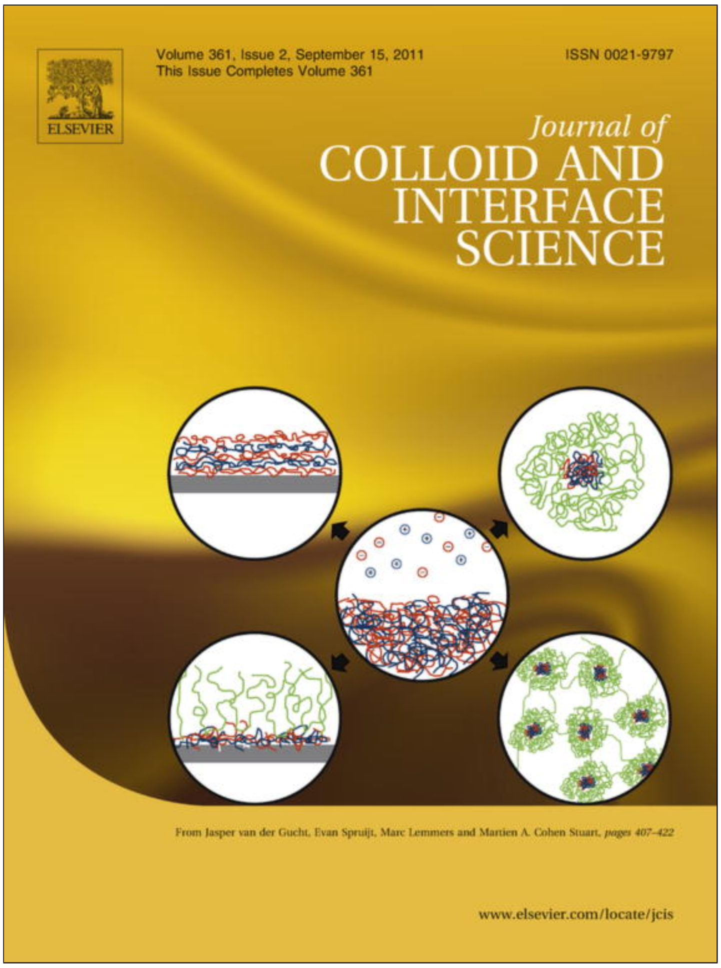

Volume 361, Issue 2, September 15, 2011
This Issue Completes Volume 361
ISSN 0021-9797
ELSEVIER
Journal of
COLLOID AND
INTERFACE
SCIENCE
From Jasper van der Gucht, Evan Spruijt, Marc Lemmers and Martien A. Cohen Stuart, pages 407–422
www.elsevier.com/locate/jcis

Journal of Colloid and Interface Science 361 (2011) 443–455

Contents lists available at ScienceDirect

Journal of Colloid and Interface Science

www.elsevier.com/locate/jcis

# Electrophoresis of concentrated colloidal dispersions in low-polar solvents

Teun Vissers [a,*], Arnout Imhof [a], Félix Carrique [b], Ángel V. Delgado [c], Alfons van Blaaderen [a]

[a] Soft Condensed Matter, Debye Institute for Nanomaterials Science, Utrecht University, Princetonplein 5, 3584 CC Utrecht, The Netherlands
[b] Departamento de Física Aplicada I, Facultad de Ciencias, Campus Teatinos, 29071 Málaga, Spain
[c] Departamento de Física Aplicada, Facultad de Ciencias, Campus Fuentenueva, 18071 Granada, Spain

ARTICLE INFO

*Article history:*
Received 7 February 2011
Accepted 27 April 2011
Available online 11 May 2011

*Keywords:*
Colloids
Electrophoresis
Low-polar
Real-space
Zeta-potential
Charge
Self-diffusion

ABSTRACT

We present a method to accurately measure the electrophoretic mobility of spherical colloids at high volume fractions in real space using confocal laser scanning microscopy (CLSM) and particle tracking. We show that for polymethylmethacrylate (PMMA) particles in a low-polar, density- and refractive-index-matched mixture of cyclohexylbromide and cis-decahydronaphthalene, the electrophoretic mobility decreases nonlinearly with increasing volume fraction. From the electrophoretic mobilities, we calculate the $\zeta$-potential and the particle charge with and without correcting for volume fraction effects. For both cases, we find a decreasing particle charge as a function of volume fraction. This is in accordance with the fact that the charges originate from chemical equilibria that represent so-called weak association and/or dissociation reactions. Finally, as our methodology also provides data on particle self-diffusion in the presence of an electric field, we also analyze the diffusion at different volume fractions and identify a nonlinear decreasing trend for increasing volume fraction.

## 1. Introduction

Colloids in nonpolar media are usually stabilized by grafting or adsorbing a polymer layer onto the particle surfaces. Short-ranged repulsive interactions resulting from the overlap of these steric layers provide stability against the attractive Van der Waals forces. However, it has long been recognized that, even in solvents of the lowest polarity, charges sometimes play an important role, despite the fact that ion concentrations are extremely low [1,2]. Well-known examples are the strong electric fields that may arise when friction causes charges to become separated during the pumping of insulating liquids or when electrically charged water droplets settle to the bottom of a container filled with petroleum products [3]. Addition of small amounts of organic salts containing large ions proves to significantly increase the conductivity, allowing the charges to dissipate sufficiently fast to prevent explosion hazard of the products. Furthermore, charged colloids can be used in xerography as an alternative to dry toning [2]. In this process, the charged particles move by electrophoresis toward a charged surface that holds a charge image. Once the particles have arrived on the surface, they form a real image on the electronic template that can be made permanent by evaporation of the solvent, leaving the particles behind. Driven by the wish to realize soft interactions for micron-sized colloids [4,5], and the design of advanced materials like electronic ink [6], interest in interactions between charged particles in nonaqueous solvents has again increased in the last decade [7–11].

The overlap of double layers can contribute significantly to the interactions between the particles as a result of long double layers in nonaqueous colloidal dispersions. In general, double layers start to overlap when the distance between two colloidal particles becomes of the same order as the Debye–Hückel screening length $\kappa^{-1}$:

$$\phi^{-1/3}a \approx \kappa^{-1}. \tag{1}$$

Already in 1948, Verwey and Overbeek calculated the free energy required to let two colloids approach each other from infinity [12]. It was found that for small surface potentials ($\zeta < 25$ mV) and moderate $\kappa a$, it hardly matters whether the charge or the surface potential is held constant during this process [12,13]. The difference between these two cases is on the order of 20% at $\kappa a = 0.1$ when the colloids are separated by a distance equal to their radius.

The low, but finite degree of dissociation of electrolytes in low-polar media causes long double layers around the colloids, ($\kappa^{-1} \gg a$) and limits the total amount of charge that builds up on the particle surface. However, since these charges are poorly screened, the double-layer interactions are long ranged and the colloids may acquire surface potentials that are similar in magnitude to those observed in aqueous dispersions [1]. Albers and Overbeek used this to explain the reduced stability of some water-in-oil emulsions at all but the lowest water volume fractions [14]: even though the electric potential is sufficiently high, the potential gradient, corresponding to the repulsive force, is low when

---

[*] Corresponding author.
*E-mail address:* t.vissers@uu.nl (T. Vissers).

0021-9797/$ - see front matter © 2011 Elsevier Inc. All rights reserved.
doi:10.1016/j.jcis.2011.04.113

the droplets are already sitting in each other's (extended) double layer. In addition, Albers and Overbeek realized that in such situations, it no longer suffices to describe the system using only pair interactions and provided a simplified model to account for multi-particle interactions.

Indirectly, the particle charge and screening length $\kappa^{-1}$ in a nondilute suspension can be estimated by measuring the radial distribution function of a particle suspension and fitting it to distribution functions from Monte Carlo simulations, assuming pairwise additivity [4,15,16]. Although this method works well for fluid suspensions, it was recently shown [17] that for an fcc crystal of the same charge-stabilized colloidal model system as studied in our paper, pairwise additivity breaks down and an effective radially symmetric pair potential does not yield an appropriate description of the system. One example of a direct measurement, again using particles and solvent similar to the present study, is given by Roberts et al. [18], where the charge on a particle can be resolved with an uncertainty of about 0.25$e$ by studying the resonance of a particle in an optical tweezer trap while it is driven by a sinusoidal field. Micron-sized polymethylmethacrylate (PMMA) particles in (dry) dodecane were found to carry on average three electron charges, but this increased to around 60$e$ when oil-soluble surfactants were added. Although the accuracy of this method is high, it can only be performed at reasonably low volume fractions. Recently, Merrill et al. measured the electrostatic forces in a many-body system at low ionic strength (PMMA particles in hexadecane) by bringing small groups of particles together using optical tweezers [19]. These data showed good agreement with a constant surface potential model, showing a decreasing charge as a function of increasing volume fraction. In strongly deionized dispersions, interactions can also become rather long ranged. Indeed, three-body interactions contribute significantly to the total interaction energy and should be taken into account [20].

Electrophoresis [21] offers another way to determine the particle surface potential and charge and we will employ it in the present paper. By measuring the electrophoretic mobility $\mu = v/E$, where $v$ is the speed of the particle moving in an electric field of strength $|E|$, the surface potential and the particle charge can be determined. Electrophoretic mobilities can be measured by laser Doppler anemometry [22] but can also be determined in real space using an optical microscope [23,24]. In this paper, we use confocal laser scanning microscopy (CLSM) and particle tracking software to obtain the trajectories of individual particles moving in an electric field. From this, we can directly obtain the electrophoretic mobility. The particles used in this work have a refractive index that is matched to the fluid mixture, which allows for measuring at different depths in the sample simply by altering the focal plane of the microscope. The optical resolution of our confocal microscope allows for the measurement of small collective particle displacements of several nanometers. This is indeed a large advantage, since in apolar solvents, the charge is generally low, resulting in small mobilities. Additionally, real-space techniques allow for obtaining three-dimensional information during the measurements. This is useful because several additional phenomena can influence the structure and local volume fraction of the dispersion [25]. For example, particle polarization can result in string formation and flows can become unstable under certain conditions. In this respect, real-space techniques offer a large advantage since the presence or absence of these phenomena can be directly observed.

The outline of this paper is as follows. Before we discuss our results, we give a short overview of the relevant theory for this paper and briefly discuss the methods that we employ. First, we determine the electrophoretic mobility $\mu$ of the colloids at different colloidal volume fractions. We compare the results from our real-space technique with measurements that we performed with the same particles using a commercially available apparatus employing Doppler anemometry. We extract the $\zeta$-potential and the surface charges $Q$ as a function of volume fraction $\phi$ using calculations of electrophoresis for concentrated colloidal dispersions [26]. We also analyze the self-diffusion of the charged particles in the electric field as our methodology to analyze the electrophoresis data in real space provided us with this information as well. We compare our results with earlier investigations and theoretical predictions.

## 2. Theory

### 2.1. Electrophoresis

When a DC field is applied on a dispersion of particles (low-$\epsilon$ solvent) free components in the system that are charged (colloids, ions, and fluid) are set into motion. For dilute systems, in the limit of thick double-layers ($\kappa a \ll 1$) the relationship between the zeta-potential $\zeta$ and the electrophoretic mobility $\mu$ is given by the Hückel equation $\mu = \frac{2\epsilon_m \epsilon_0 \zeta}{3\eta}$, where $\epsilon_m$ is the relative permittivity, $\epsilon_0$ the permittivity of vacuum, and $\eta$ the viscosity. In the limit of thin double layers ($\kappa a \gg 1$), the electrophoretic mobility is given by the Smoluchowski equation $\mu = \frac{\epsilon_m \epsilon_0 \zeta}{\eta}$.

Since Hückel and Smoluchowski did not include deviations of the local electric field from the applied field, the above formulas do not predict the situations for intermediate $\kappa a$ correctly. It was demonstrated by Henry [27] that, when taking into account the local electric fields around the particles, by superimposing the external electric field on the particle's electric field, the electrophoretic mobility can be written as $\mu = \frac{2\epsilon_m \epsilon_0 \zeta}{3\eta} \cdot f_1(\kappa a)$ where $f_1(\kappa a)$ is given by Henry's function [27,28], which approaches 1 and 3/2 for small and large $\kappa a$ respectively, in line with the Hückel and Smoluchowski limits. The charge can be calculated from the $\zeta$-potential using for example the relationship by Loeb et al. [29].

In order to find solutions for any $\kappa a$ and any $\zeta$-potential, it is necessary to take into account geometrical effects and the correct ion distribution around the particle (this distribution is influenced by the fluid flow and the electric field). To accomplish this, in general, a set of partial differential equations must be solved for the local ion density, ion fluxes, and the fluid flows around the colloid. Analytical solutions were obtained by Overbeek [30] in 1943 and by Booth in 1950 [31], by expressing the mobility as a power series in $\zeta$ and evaluating the first few coefficients. Later, Wiersema [32] and O'Brien and White [33] used numerical calculations to relate the $\zeta$-potential to the mobility $\mu$. These results, and their comparison with analytical expressions, are treated extensively by Hunter [34].

### 2.2. Effects of volume fraction on the electrophoretic mobility

When suspensions become more concentrated, the particles start to interact with each other. In systems where a high degree of ionic screening is present ($\kappa a \gg 1$), the double layer is very thin compared to the particle radius. Therefore, charge separation only occurs in the double-layer region around the particle. Net electric forces exerted by an external field will therefore only act on this region, resulting in strongly screened hydrodynamic and electrostatic interactions [35]. It was shown both theoretically [36] and experimentally [37] that the electrophoretic mobility shows a weak concentration dependence, which results from the back flow of fluid that is caused by the motion of the particles:

$$\mu = \mu_0(1 - C\phi) + \mathcal{O}(\phi^2). \tag{2}$$

Here, $\mu_0$ is the electrophoretic mobility at infinite dilution, $C$ is a constant that is close to unity and $\mathcal{O}(\phi^2)$ denotes second-order terms. Recently, Pérez et al. confirmed this for particles suspended in an apolar solvent with added salt ($\kappa a \gg 1$) [38]. Medrano et al. showed that for longer screening lengths ($\kappa a \approx 0.44$), the dependence of the mobility on the concentration is much stronger due to particle interactions, with the constant in Eq. (2) found to be $C = 8 \pm 2$ [39]. In a paper by Lobaskin et al. [40], the electrophoretic mobility of aqueous colloidal dispersions in the low-salt regime was studied with a combination of Lattice-Boltzmann and Molecular Dynamics (LB-MD) computer simulations and laser Doppler velocimetry experiments that also shows a nonlinear decrease in the mobility with increasing volume fraction.

In the case of very low bulk ion concentrations and extended double layers ($\kappa a \ll 1$), the dependence of various dispersion parameters such as charge and surface potential on volume fraction becomes important and has been the subject of several experimental and theoretical studies. The first mobility expression for spherical particles at low $\zeta$-potentials and arbitrary double-layer thickness was derived by Levine and Neale [41] using the Kuwabara cell model [42]. Kozak and Davies generalized this theory for arbitrary values of the $\zeta$-potential. A paper by Ohshima [43], which gives the mobility for a swarm of spherical particles, also covers the limiting cases from these earlier works. The effect of charge regulation, by means of ion exchange with the fluid, on the electrophoretic mobility and the particle surface potential in highly concentrated suspensions was studied in more detail by Hsu et al. [44]. Since surface charge density can change as a result of a different degree of dissociation of charge carrying groups, both the surface charge and potential are allowed to change with the screening parameter $\kappa a$ and volume fraction $\phi$. It is shown that the surface potential decreases for increasing $\kappa a$. Also, a decreasing trend of the electrophoretic mobility with increasing volume fraction is predicted. The polarization of the double layers becomes more significant for higher surface potential, but completely vanishes when $\kappa a \to \infty$. The first theoretical work on the electrophoretic mobility of spherical colloidal particles at high concentrations for arbitrary $\zeta$-potentials that fully takes into account overlapping double layers was given recently [26]. These calculations use a Kuwabara cell model to relate the $\zeta$-potential and surface charge for arbitrary $\kappa a$ and $\phi$ to the electrophoretic mobility $\mu$. The effect of overlapping double layers on the electrophoretic mobility and the choice of appropriate boundary conditions is treated in more detail in [45].

In this paper, we measure the conductivity and mobility as a function of volume fraction of PMMA particles in a low-polar solvent mixture of cis-decalin and CHB using confocal laser scanning microscopy. We focus on the cases where the field strength is sufficiently low to ensure that particle polarization does not have an important effect on the structure of the suspension. We use calculations on electrophoresis that correct for the effect of volume fraction [26] to calculate the charge and surface potential on the particles.

### 2.3. Diffusion coefficients

Since we obtained the trajectories of the charged particles from our electrophoresis measurements, we can also study the self-diffusion in an electric field. Self-diffusion relates to the diffusional properties of individual particles and is different from, for instance, collective diffusion which is the response of a dispersion to concentration gradients. Whenever we mention in the following of the paper diffusion, we mean self-diffusion. The diffusion of charged particles with double layers larger than the particle size has been studied theoretically [46–48] and we will qualitatively compare the results with our experiments in Section 4.4.

In the most simple case of independent Brownian particles at infinite dilution, the particles do not influence each other and the diffusive motion of particles is given by:

$$\langle (\Delta r)^2 \rangle = 6 D_0 \Delta t \quad \Delta t > \tau_{\mathrm{B}}, \tag{3}$$

where $\tau_{\mathrm{B}}$ sets the Brownian time scale and $D_0$ is the single particle diffusion coefficient given by the Stokes–Einstein relation:

$$D_0 = \frac{k_B T}{6\pi\eta a}, \tag{4}$$

where $k_{\mathrm{B}}$ is the Boltzmann constant, $T$ is the temperature, $\eta$ is the dynamic viscosity of the solvent, and $a$ is the radius of the particle. When more particles are present, the diffusion of the charged particles is influenced by a combination of hydrodynamic, electrostatic, and direct interactions. The time scale on which a particle feels a change in configuration is set by the interaction time scale $\tau_I$. Since the double layers can interact as well, $\tau_I \propto a^2/D_0$ will be shorter for soft spheres than for hard spheres.

For short time intervals $\tau_B < \Delta t < \tau_I$, the particles move in a nearly constant configuration of neighboring particles and only experience hydrodynamic interactions. In this regime, the mean-square displacement and time are related to the short-time self-diffusion coefficient:

$$D_S = \frac{\langle (\Delta r(\Delta t))^2 \rangle}{6\Delta t} \quad \tau_{\mathrm{B}} < \Delta t < \tau_{\mathrm{I}}. \tag{5}$$

On the other hand, if $\Delta t \gg \tau_{\mathrm{I}}$, the mean-square displacement is a result of the combined effect of hydrodynamic, electrostatic, and direct interactions (the particles cannot penetrate each other and interact through their interparticle potential). The mean-square displacement and time are related to the long-term diffusion coefficient:

$$D_L = \lim_{\Delta t \to \infty} \frac{\langle (\Delta r(\Delta t))^2 \rangle}{6\Delta t} \quad \tau_{\mathrm{I}} \ll \Delta t. \tag{6}$$

For intermediate time scales $\tau_{\mathrm{S}} < \Delta t < \tau_{\mathrm{I}}$ on which the particle interactions cannot be averaged over all possible configurations within that time, the mean-square displacement is not a linear function of time and the diffusion coefficient is not a constant. For these intermediate time scales, an apparent diffusion coefficient can still be defined:

$$D(\Delta t) = \frac{\langle (\Delta r(\Delta t))^2 \rangle}{6\Delta t} \quad \Delta t \approx \tau_I, \tag{7}$$

which is a function of the time interval $\Delta t$ over which it was measured. The diffusion of charged particles while they are also driven by an electric field is studied in Section 4.4.

## 3. Methods

### 3.1. Particle dispersions

Polymethylmethacrylate (PMMA) particles were synthesised by dispersion polymerization [49]. The particles were covalently labeled with either 7-nitrobenzo-2-oxa-1,3-diazole (NBD) or rhodamine B isothiocyanate (RITC) [49]. The colloids were sterically stabilized with a graft-poly-12-hydroxystearic acid PHSA–PMMA-comb stabilizer. In all cases, the stabilizer was covalently linked to the particle surface after the synthesis. After this step, the particles were washed with hexane several times to remove unreacted monomer and consequently dried by letting the hexane evaporate in air. The particle size and polydispersity were determined by static light scattering (SLS). For the electrophoresis measurements, we used two different particle batches **A** (average diameter $\sigma_{\mathbf{A}} = 1.06$ μm, 6% polydispersity, NBD-labeled) and **B** ($\sigma_{\mathbf{B}} = 0.91$ μm, 7% polydispersity, RITC-labeled). In addition, particles **N** ($\sigma_{\mathbf{N}}$ = 2.05 µm, 4% polydispersity, RITC-labeled) were used for conductivity measurements. Suspensions at different volume fractions containing either particles **A** or particles **B** were prepared by dispersing colloids in a mixture of 27.2 w% cis-decahydronaphthalene ('cis-decalin') and 72.8 w% cyclohexylbromide (CHB). In this solvent mixture, the density and refractive index of the background and the colloids are nearly matched. After dispersing the particles, they were allowed to equilibrate in CHB/cis-decalin for a period of at least three days prior to the electrophoresis measurements.

### 3.2. Electrophoresis

After the equilibration period, the particle dispersions were transferred to rectangular glass capillaries (Vitrocom 0.1 × 2.0 mm) with electrodes connected on both ends of the capillary (Fig. 1). We verified that no air bubbles emerged inside the dispersion in the capillary during this procedure. The capillaries were then sealed with either wax or UV-glue (Norland optical adhesive). In the latter case, the glue was cured with UV-light ($\lambda$ = 350 nm, UVGL-58 UV lamp, UVP) for approximately 30 min. During this curing process, the capillaries were covered with aluminum foil to shield the suspension inside the sample and protect it from the UV radiation. Since the electric cells could not be reused, we prepared a new one for each volume fraction. All electrophoretic profiles were measured on a Leica SP2 confocal microscope (using a 488 nm or 543 nm laser), using an NA 1.3 40× oil-immersion objective (Leica). For the generation of the electric fields, a wideband amplifier (Krohn-Hite, Model 7602M) was used. The electric field was applied in the $x$-direction (Fig. 1). Measurements were performed in the middle between the electrodes and at the center of the capillary channel in the $y$-direction. We used a so-called dial-indicator (Schut) that measures micrometer scale displacements to locate the center of the capillary in the $y$-direction ($y = 0$).

In electrophoresis measurements, the electrophoretic velocity should be measured at the stationary layers (Eq. 9), where the fluid flows resulting from electro-osmosis on the walls of the capillary channel cancel each other. To increase the accuracy of the measurement, we recorded movies for a number of different depths (more than 5 in all cases) along the vertical ($z$)-axis of the capillary. Then, we fitted the resulting velocity profile to a parabolic function, to obtain the velocity at the stationary layers [22]. After mounting the sample on the stage, the location of the lower and upper glass walls was determined using the $z$-stage on the confocal microscope. From this, the distance $h$ between the capillary walls in the $z$-direction, which varied about 10–30% for different capillaries, was determined for each individual sample. Occasionally, capillary effects acting on the immersion oil droplet between the objective and the capillary caused a small drift of the sample in the $z$-direction. This drift was taken into account by assuming that the extremum in the Poiseuille flow (PF) profile was always located exactly in the center of the capillary channel in the $z$-direction ($z = 0$).

Images were recorded at a resolution of 512 × 512 or 1024 × 1024 pixels, at a scanning speed of approximately 2–3 frames per second. To determine the particle positions in each frame, we used algorithms similar to [50]. We used Gaussian blurring to smoothen the intensity landscape and reduce noise. To correct for background noise, we occasionally used a top hat filter. The particle trajectories were determined using the 2D tracking algorithms described in the next section.

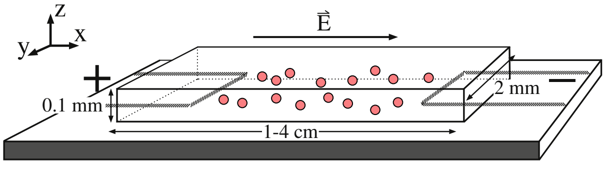

**Fig. 1.** A schematic 3D view of a rectangular glass capillary with cross-section dimensions 0.1 mm × 2 mm. After a dispersion was transferred into the capillary, conducting wires bent at an angle were inserted as electrodes at both ends of the capillary. The capillary itself was closed at both ends with either UV-glue or wax. Black lines represent the conducting wires.

### 3.3. Particles moving uniformly in an electric field

To estimate the charge on the particles, it is required to obtain the electrophoretic mobility $\mu = v/E$ of the particles, where $v$ is the electrophoretic velocity and E the electric field strength. To determine the electrophoretic velocity, we need to identify the moving particles in different frames to construct their trajectories. To do this, we cannot simply apply the existing tracking algorithm described above, since in our confocal setup already for moderate driving fields $E$ the average particle displacements in the field direction can exceed the typical spacing between the colloids $d$, resulting in wrong particle identifications.

We demonstrate that particles can still be correctly identified, if first an estimate is made of the average displacement in the field direction. To do this, we make use of the fact that the drift velocity at a depth $z$ in the middle of the capillary channel is similar for all particles so that the particles move uniformly in one direction. First, an estimate of the uniform displacement $\langle\Delta\mathbf{R}\rangle$ between successive frames is made. Subsequently, we add this average displacement to a particle in a given frame to match it with a particle in the next frame. We make use of the fact that if we add the correct uniform displacement to the particles in frame $m$, the total mean-square displacement over all particles to their nearest particles in frame $m + 1$ will be minimal. If the field is applied along the $x$-direction, we can minimize the total mean-square distance to nearest neighbors in the next frame with respect to the estimated displacement $\Delta x$. This total mean-square displacement for a displacement $\Delta x = \Delta\mathbf{R}\cdot\hat{x}$ is given by:

$$\xi(\Delta x) = \frac{1}{N_m}\sum_{i=0}^{N_m}\left(\mathbf{R}_{i,m}\cdot\hat{x} + \Delta\mathbf{R}\cdot\hat{x} - \mathbf{R}_{j,(m+1)}\cdot\hat{x}\right)^2 \qquad (8)$$

where $\mathbf{R}_{i,m}$ is the position of particle $i$ in frame $m$. $\Delta\mathbf{R}\cdot\hat{\mathbf{x}}$ is here taken along the $x$-axis but it could be taken along any direction in the plane. $\mathbf{R}_{j,m+1}$ is the position of particle $j$ in frame $m + 1$ that is nearest to the displaced particle $i$. Particle $j$ should be located within a circle with a well-defined critical radius $r_c$ around the displaced particle $i$. $N_m$ is the total number of particles in frame $m$ that has at least one particle in frame $m + 1$ that is closer than $r_c$ (after adding the estimated displacement to the particles in frame $m$).

We recorded a series of images of particles **B** moving uniformly in an electric field. For this dataset, we plotted Eq. (8) in Fig. 2. From the minimum in $\xi(\Delta x)$, we estimate the uniform displacement $\langle\Delta x_{\mathrm{est}}\rangle = -1.226$ µm. First, this estimate was added to all the particle positions in frame $m$. Subsequently, the particles were matched with particles in the next frame $m + 1$ by means of the conventional 2D tracking algorithm. The resulting average displacement $\langle\Delta x\rangle$ along the field direction between two consecutive frames was thus refined to −1.215 µm. Recently, we became aware of a paper that calculates the cross-correlation function for two successive frames to estimate the uniform displacement as in a sheared suspension [51]. Their method is similar to the one we used here, but uses the correlation between all the pixels in consecutive frames instead of already determined particle coordinates.

### 3.4. Testing the particle tracking algorithm

In the confocal microscopy experiments, the particles could diffuse in and out of the diffraction-limited optical slice that defined

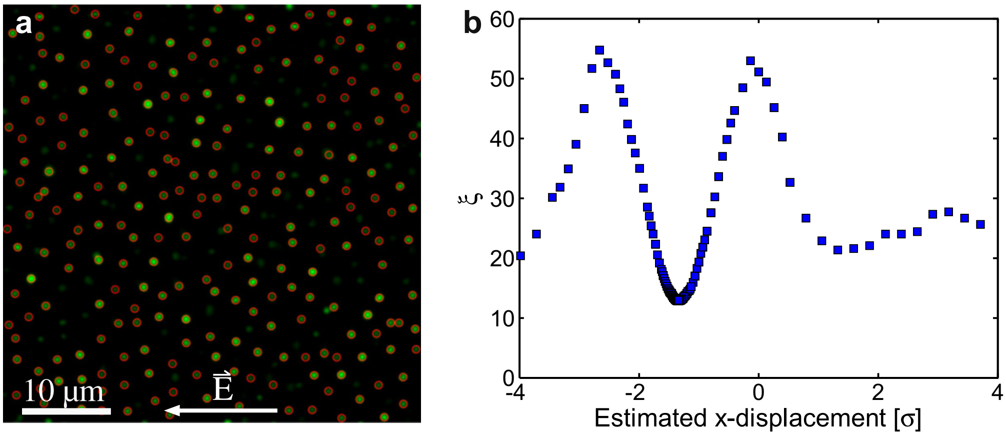

**Fig. 2.** (a) Confocal images (taken in the $(xy)$-plane) of particles **B** ($\phi = 0.02$). The electric field is in the horizontal direction. The red circles mark particles recognized by the tracking algorithm. (b) $\xi$ (Eq. (8)) for particles **B** at $\phi = 0.02$ moving in an electric field (2.65 V/mm). The value for $\xi$ is minimum for a displacement of $\Delta x_{est} = -1.226$ µm. Using this estimate, we determined the average displacement after identification of all the particles at −1.215 µm. (For interpretation of the references to color in this figure legend, the reader is referred to the web version of this article.)

our field of view. Inevitably, this occasionally resulted in incorrectly identified particles. To estimate the number of incorrectly matched particles between the frames, we used data from Brownian dynamics computer simulations in which the particles are driven by an electric field.

In these simulations, each particle had a unique ID number. To mimic the experimental reality, we only saved the $x$-and $y$-coordinates and the unique particle ID of particles inside a slice out of the simulation box that was oriented in the $(xy)$-plane with a thickness $\Delta z = 1.6$ µm and used these data as input for the particle tracking algorithm. The particle IDs allowed us to detect falsely identified particles, for which the results are shown in Fig. 3. The number of incorrectly identified particles increases with $\phi$ but does not depend on the field strength since in the simulations the particles moved uniformly. Naturally, the larger the Brownian motion, the more uncertain the results of the tracking will be. In these tests, we used a scanning speed of 5 frames per second and the mean-square fluctuations between two consecutive frames were between 0.04 and 0.15 µm$^2$, which is close to the values in this work. In reality, the error could depend on the field strength in the case that there is a breakdown of uniform movement. We compared the particle displacements and diffusion coefficients from the simulation with the values found by our particle tracking algorithm. The errors in the drift velocity were typically less than 1%. The errors in the diffusion coefficients were larger, typically around 10%. Hence, we can be confident that we can accurately determine the electrophoretic mobility of a uniformly moving concentrated colloidal suspension. For the determination of the self-diffusion constant, care should be taken, since the values can deviate if the number of wrongly identified particles becomes large.

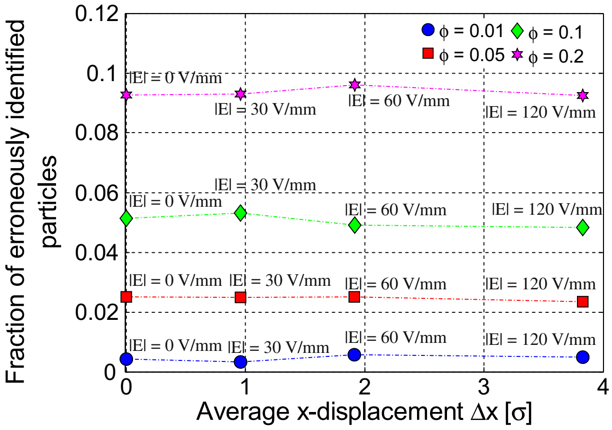

**Fig. 3.** The fraction of erroneously identified particles between successive frames obtained from testing our tracking algorithm with Brownian dynamics computer simulations data of colloids ($\sigma = 0.93$ µm) moving in an electric field with field strength $|E|$. Note that the actual magnitude of the uniform displacement does not change the fraction of falsely matched particles, although the time interval (and hence the mean-square particle displacements) between two successive frames was the same for all field strengths. The depth of the slice, used to mimic the 'optical depth' in the experiments, was 1.6 µm.

### 3.5. Doppler velocimetry measurements

In addition to the confocal microscopy measurements, we also determined the electrophoretic mobility using a Zetasizer Nano (Malvern(UK)) apparatus. To do this, the equilibrated samples were transferred into a glass cell (12 mm square glass cell PCS1115, Malvern) after which the electrophoretic mobility was measured using a probe that is suitable for organic solvents (universal dip cell PCS1115, Malvern).

### 3.6. Conductivity measurements

The conductivity of both the pure CHB/cis-decalin mixture and the suspensions with particle **A** in CHB/cis-decalin were measured with a Scientifica (UK) model 627 conductivity meter.

## 4. Results & discussion

### 4.1. Conductivity of the suspensions

We study the conductivity of the suspension for different volume fractions $\phi$ of two different particle species, namely **A**, ($\sigma_{\mathbf{A}} = 1.06$ µm) and **N** ($\sigma_{\mathbf{N}} = 2.05$ µm). Since a relatively large quantity of suspension (approximately 4 mL for each measurement) was required to obtain the conductivity $\sigma^c$, we started with a concentrated suspension of particles and diluted this after each measurement to obtain the conductivity curve $\sigma^c(\phi)$. For our suspension conductivity measurements, we used 3 different batches (with different treatment, suppliers, and/or shelf-times) of cis-decalin (27.2 w%) in CHB that we labeled $\alpha$, $\beta$, $\gamma$ and $\delta$. In the case of batch $\alpha$, molecular sieves were added during the purification to lower the conductivity from 115 pS/cm to 2.3 pS/cm. Batches $\beta$ and $\gamma$ were obtained by mixing as received CHB with

**Table 1**
Measured conductivities of different batches of cis-decalin (27.2 w%) in CHB without any colloids added. For each batch the origin of the CHB and the date that the bottle was received are also given.

| Batch | $\alpha$ | $\beta$ | $\gamma$ | $\delta$ |
|---|---|---|---|---|
| $\sigma^c$ (pS/cm) | 2.3 | 51 | 272 | 263 |
| CHB: | Fluka purified | Sigma–Aldrich as rec. | Fluka as rec. | Sigma–Aldrich as rec. |
| CHB received | March 2008 | April 2009 | March 2008 | October 2007 |

cis-decalin, without any purification steps. The initial conductivities were measured for each batch and are summarized in Table 1.

For particles **A** in solvent $\beta$, the conductivity initially drops and then increases again with approximately a factor 3 to reach a level of approximately 120 pS/cm. The initial drop at low concentrations could be caused by the effect of adding insulating PMMA particles to the solvent mixture, in this case lowering the conductivity of the dispersion as a whole. Interestingly, something different happens with particles **N** in solvent $\gamma$; as the volume fraction increases, the conductivity decreases to approximately the same plateau as for particles **A** in solvent $\beta$. Evidence that the particles can indeed enhance the concentration of ions in the solution is given by studying particles **A** and **N** in the purified solvent batch $\alpha$. The increase in conductivity with the particle volume fraction suggests that the particles themselves introduced new ions or that they increased the degree of ion dissociation by the presence of polar groups at the surface of the particle.

To determine the origin of the ions upon addition of colloids, we used a suspension of colloids **N** in solvent $\alpha$ ($\phi = 0.1$) with a measured conductivity of $\sigma^c = 75.5$ pS/cm. After sedimenting the particles by centrifugation, we determined that the conductivity of the supernatant had a comparable value of $\sigma^c = 81.4$ pS/cm. This measurement suggests that the ion concentration did not only increase in the double layer around the colloids, but also in the bulk solution. This suggests the possibility that the ion concentration was increased as a result of species that were introduced by the particles. These substances could have originated from the stabilizer that was adsorbed to the particle surface. To confirm this, we completely dried the (PHSA)–PMMA-comb stabilizer and washed it three times with hexane (same treatment as the particles with stabilizer on them receive after their synthesis and before dispersing them in CHB/cis-decalin) to remove remains of toluene, ethyl acetate, butyl acetate, and other (polar) substances. After this step, we saturated the mixture of cis-decalin (27.2 w%) and CHB ($\sigma^c = 34$ pS/cm) with the remaining stabilizer and measured the conductivity of the viscous mixture of solvent and (PHSA)–PMMA-comb stabilizer ($\sigma^c = 315$ pS/cm). Although free stabilizer is not the same in composition as stabilizer adsorbed to the particle surface, this measurement seems to confirm that compounds in the stabilizer can be a source of extra ions.

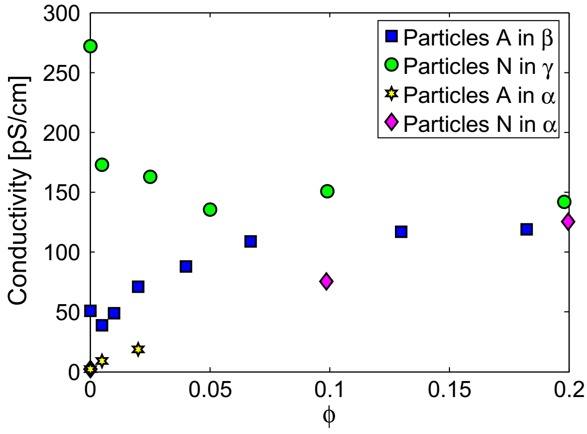

**Fig. 4.** Measured conductivities as a function of volume fraction $\phi$ for several different systems containing either particles **A** or **N** and solvent batch $\alpha$, $\beta$ or $\gamma$.

Generally, it can be said that there is a dissociation/association equilibrium of ions near the surface of the colloid. By adsorbing ions from the bulk solvent, it is possible that chemical equilibria inside the solvent are shifted to generate new ions, leading to an increase in the conductivity. In addition, it is possible that the colloids *themselves* can introduce new ions to the suspension or enhance the concentration of ionic groups.

For the electrophoresis experiments in this paper, particles **A** and **B** were dispersed in a mixture of cis-decalin (27.2 w%) in CHB (batch $\delta$) that has an initial conductivity of 263 pS/cm, corresponding to $\kappa^{-1} \approx 1$ µm. Unfortunately, we did not have a sufficient amount of colloids to perform the conductivity experiments for these particles in solvent mixture $\delta$. From the conductivity measurements of particles **N** in batch $\gamma$ (Fig. 4), it seems reasonable to assume that the screening length $\kappa^{-1}$ again remains relatively constant for increasing particle volume fraction.

### 4.2. Electrophoresis measurements

In this section, we describe our electrophoresis measurements of the colloidal dispersions **A** and **B**. First, we present our measurements of the electrophoretic mobility $\mu = v/E$. Subsequently, we use this quantity to calculate the charge and the $\zeta$-potential of the colloidal particles.

To calculate the mobility $\mu$ from our data, we extracted the trajectories of particles from a sequence of frames that we obtained using the confocal microscope and applying the tracking algorithms described in Section 3.3. In Fig. 5, a few examples are depicted in the experimental data obtained for particles **B**. Fig. 5a shows trajectories for colloids **B** at a volume fraction of $\phi = 0.35$ when no field was applied and only Brownian motion was observed. In Fig. 5b, an electric field was present, resulting in the uniform motion of colloids in the direction of the field (horizontal). Fig. 5c shows something similar as in Fig. 5b, for particles **B** in a dilute suspension ($\phi = 0.0026$). The particle trajectories have a limited length, since the particles can diffuse in and out of the optical slice that defines our field of view, causing the particles to move out of sight after some time. Fig. 5d shows the distribution of the trajectory lengths, which confirms this. From each particle trajectory, we obtained the velocity of a particle, from which the mobility was calculated in turn. The result was then averaged over all particles. To ensure the reliability of our data, we only used trajectories of particles that could be identified for more than 5 consecutive frames in our calculation.

When an electric field is applied in a closed capillary, counterions near the charged wall are set in motion and drag along the fluid, resulting in an electro-osmotic plug flow (EOF). Since the fluid is incompressible, a counterpressure builds up and a parabolic Poiseuille flow (PF) ensues in the opposite direction to cause a zero net flow. Both flows exactly cancel at the stationary layers, which for our rectangular capillary (Fig. 1) are located at [34]:

$$\frac{z_{\mathrm{stat}}}{h} = \sqrt{\frac{1}{3} + 4\left(\frac{2}{\pi}\right)^5 \frac{1}{k}}, \qquad (9)$$

where $k$ is the ratio between the major and minor cross-section of the capillary, $h$ is the distance in the $z$-direction from the center of the channel to either of the walls, and $z_{\mathrm{stat}}$ is the distance in the $z$-direction from the center of the channel to one of the stationary layers (for $y = 0$, where our measurements were performed). For example, for a capillary with $h = 61$ µm, $z_{\mathrm{stat}} \approx \pm 36.3$ µm ($k \approx 20$). To calculate the electrophoretic mobility $\mu$ of the particles at the stationary layers, the electrophoretic mobility was measured for

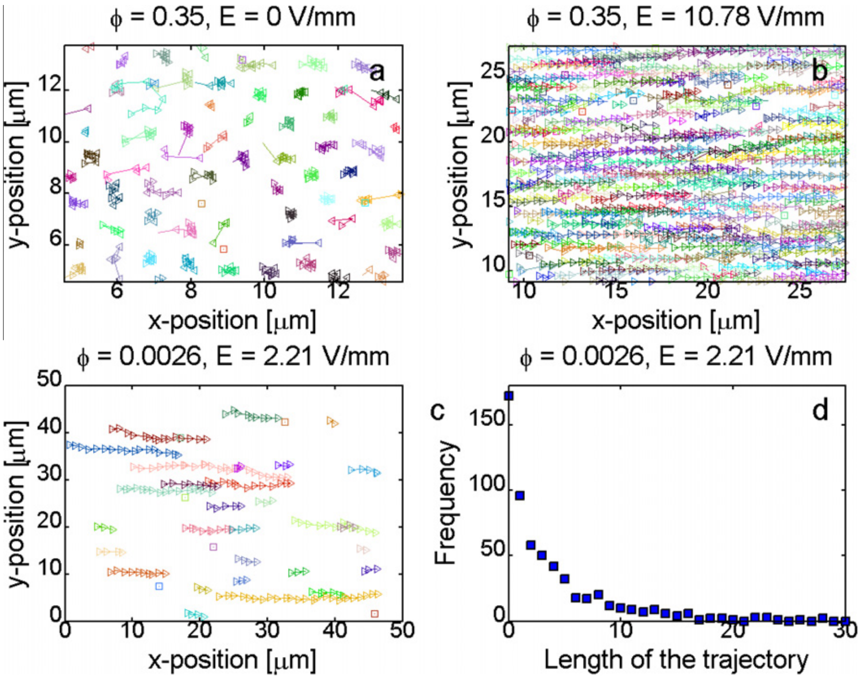

**Fig. 5.** Particle trajectories, the direction of movement is given by the orientation of the triangles. (a) Trajectories for particles **B** at $\phi = 0.35$ in the (*xy*)-plane, at zero E-field. (b) Trajectories for particles **B** at $\phi = 0.35$, and $|E| = 10.78$ V/mm. (c) Trajectories for particles **B** at $\phi = 0.0026$, and $|E| = 2.21$ V/mm. Only trajectories starting at $t = 0$ are shown for at most the next 10 frames (a and b) or at most the next 80 frames (c). (d) The distribution of the trajectory lengths for particles **B** at $\phi = 0.0026$, and $|E| = 2.21$ V/mm. The frame rates were either 1.35 $s^{-1}$ (a) or 2.37 $s^{-1}$ (b and c).

several depths $z$ and fitted to a parabola [22]. By evaluating this parabola at $z = \pm z_{stat}$, the mobility at the stationary layer was obtained.

For both particle batches **A** and **B**, the mobility was determined as a function of the channel depth $z$ for volume fractions in the range of $\phi = 0.001–0.35$. In Fig. 6, the electrophoretic mobility profile along the $z$-direction of the channel is given for particles **B** at $\phi = 0.02$ (Fig. 6a) and $\phi = 0.13$ (Fig. 6b). The blue vertical lines depict the upper and lower glass walls of the capillary. The magenta vertical lines denote the positions of the stationary layers. The positive mobility at the stationary layers indicates that the particles were positively charged. We have verified that the mobility did not change significantly with the field strength for all measurements where $\phi \leqslant 0.3$ and $|E| < 20$ V/mm, indicating a linear field dependence of the velocity $v = \mu E$. In one measurement (particles **B** at $\phi = 0.35$), already a large amount of local order was present, suggesting that the suspension was close to crystallization. Moreover, the mobility profile did in this case change for different field strengths.

We noticed an unusual change of direction of the EOF at the lowest volume fractions while studying $\mu$ as a function of $\phi$. The mobility profiles for particles **A** at $\phi = 0.001$ and $\phi = 0.0025$ demonstrate this (Fig. 7a and b respectively). At the stationary plane, $\mu$ has a positive value for both volume fractions, showing that the particles moved toward the negative electrode and were therefore positively charged. Also, for both suspensions, we observed the adsorption of particles to the upper and lower glass walls of the capillaries. The adsorption of particles is only expected if the sign of the particle charge is opposite to the charge sign of the wall, indicating that the bare wall charge was initially negative.

For $\phi = 0.0025$, the Poiseuille flow (PF) is directed in the same direction as the particle movement. Recall that in a closed capillary, a PF arises to counteract the EOF that was caused by negatively charged ions on the wall. Hence, the capillary walls are positively charged for $\phi = 0.0025$. On the other hand, for $\phi = 0.001$, the PF counteracts the direction in which the particles move, meaning that the capillary walls are negatively charged (the EOF is caused by moving positively charged ions). Hence, we conclude that particle adsorption reverses the net charge on the capillary wall and thus also reverses the direction of the EOF and PF.

Since a significant fraction of particles was adsorbed to the walls at these low volume fractions, the actual volume fraction inside of the capillary was lower than for the prepared suspensions. For the higher volume fractions $\phi > 0.01$, this effect was relatively small, but in the cases where the volume fraction was very low, this was certainly not the case. At $\phi = 0.001$, the volume fraction of particles kept decreasing in time, until all free particles were stuck to the wall (no particles were observed in the suspension anymore). The upwards shift of the mobility profile going from 2.28 V/mm to 5.54 V/mm for $\phi = 0.0025$ was probably due to ongoing particles adsorption in the time between the two measurements, lowering the effective volume fraction and increasing the particle mobility.

In Fig. 8, the stationary mobilities $\mu$ are depicted as a function of the volume fraction $\phi$ for species **A** and **B**. It is observed that both particle batches exhibit a similar trend of nonlinear decreasing mobility $\mu$ with increasing volume fraction $\phi$. The $\phi$-dependence is much stronger than for particles with thin double layers [37,39]. For particles **A** and volume fraction $\phi = 0.01$, the electrophoretic mobility shows a sudden dip. Since we do not observe a similar dip for particles **B**, it is likely that this is an outlier that is caused by an unknown external factor.

In order to compare our measurements with an independent method we have also performed mobility measurements on particles **B** with the ZetaSizer Nano (Malvern) which uses laser Doppler anemometry [52,53] to measure electrophoretic mobilities. First, the electrophoretic mobility was measured directly at the stationary layers for an applied DC electric field. Second, the mobility was measured in a low-frequency AC field, where electro-osmosis is suppressed [54]. The mobility data (Fig. 8) show roughly the same trend as observed with the CSLM method. However, the variance in

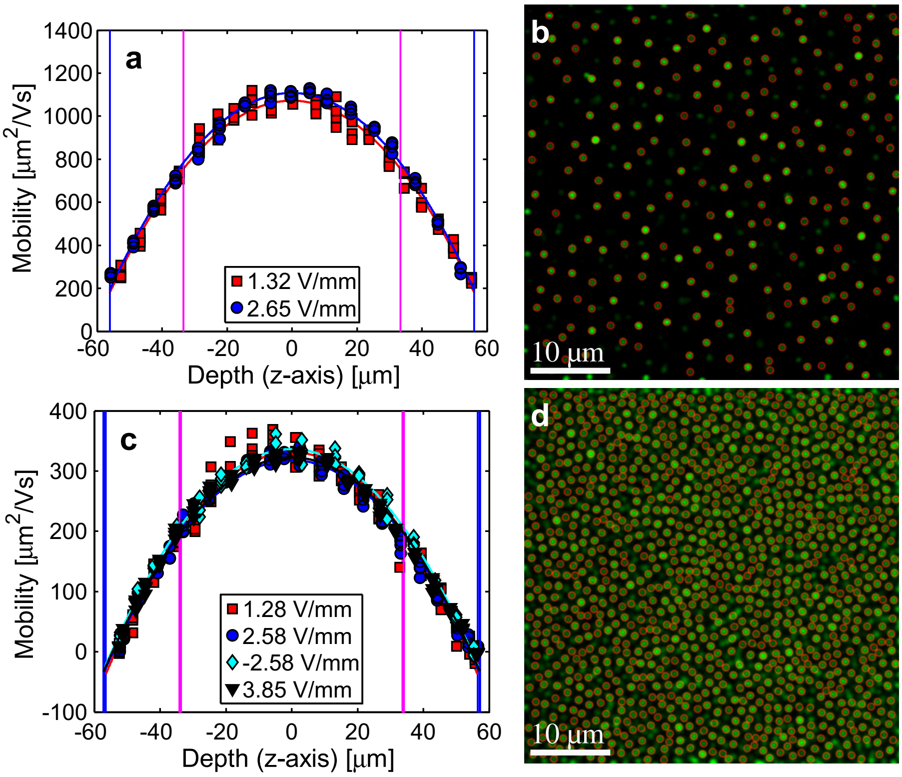

**Fig. 6.** Confocal images (taken in the ($xy$)-plane) and mobility profiles along the $z$-axis measured for (a and b) particles **B** at $\phi = 0.02$ at two different field strengths $E = 1.32$ V/mm (□) and $E = 2.65$ V/mm (○), and (c and d) particles **B** at $\phi = 0.13$ at 1.28 V/mm (□), 2.58 V/mm (○), −2.58 V/mm (◇) and 3.85 V/mm (▽). The plots show that for these low fields, the electrophoretic mobility $\mu$ does not depend on the sign nor the magnitude of the applied electric field. Blue vertical lines depict the upper and lower glass walls of the capillary. The magenta vertical lines denote the stationary planes. The red circles in the images mark particles recognized by the tracking algorithm. The center of the capillary is located at $z = 0$. (For interpretation of the references to color in this figure legend, the reader is referred to the web version of this article.)

the measured mobilities is larger than for the confocal microscope measurements especially at low volume fractions. It is likely that the precision of the method is lower, in particular for dilute systems, since the refractive index of our particles is very close to that of the solvent, and the ZetaSizer Nano uses scattered light. Additionally, it is likely that the apparatus is not sensitive enough to pick up the small Doppler shifts associated with the small speeds at which our particles travel.

### 4.3. Surface potential and charge

In this section, we use the measured electrophoretic mobilities to calculate the charge and surface potential. Several factors contribute to the strong decrease of the mobility with volume fraction. There is a $(1-\phi)$-dependence due to the fluid back flow [36,37,39] when the colloids translate and a factor $(1-\frac{\phi}{2})$ due to the lowering of effective electric field strengths in a medium containing insulating, weakly charged particles [55]. There are also hydrodynamic effects arising from the overlap of electric double layers. This in turn has effects on the local field, the ion distribution around the colloids, and thus on the hydrodynamics. These effects can all be accounted for by numerical calculations used in modern theories of electrophoresis. Here, we employ the calculations described in [26], which are designed to relate the electrophoretic mobility to the $\zeta$-potential for arbitrary double-layer thickness. We do not consider the effect of a dynamic Stern layer here. Since the polymer layer that provides steric stabilization is very small with respect to the particle diameter, we consider our particles to be rigid spheres. The calculations use a Kuwabara cell model [42], where each particle of radius $a$ is defined inside a cell with radius $b$ to model a concentrated suspension. The boundary condition for the potential at the slipping plane, chosen at $r = a$, is given by:

$$\zeta = \Psi^0(a). \tag{10}$$

Moreover, a local potential minimum is present in the middle between two neighboring particles $r = b$:

$$\left[\frac{d\Psi^0}{dr}\right]_{r=b} = 0, \tag{11}$$

where $b$ denotes the outer boundary of the cell. For all calculations, we used a dynamic viscosity of the solvent of $\eta = 2.726 \times 10^{-3}$ Pa/s, a bulk conductivity of 263 pS/cm, a dielectric constant of the solvent mixture of $\epsilon_m = 5.6$, and a dielectric constant of the particles of $\epsilon_m = 2.6$. The conductivity measurements suggest that there are no dramatic changes in the ion concentration (Section 4.1). However, we do acknowledge that the ionic strength of the dispersion might have changed with increasing volume fraction since the dependence of the conductivity on the volume fraction is in this case not yet fully understood. For this reason, we performed the calculations not only with a constant $\kappa a = 0.5$ (based on the conductivity of the solvent mixture at infinite dilution) but also for several different $\kappa a \in [0.3, 0.7]$. In addition, we performed the calculations without taking the volume fraction effects into account by filling in a very low value for $\phi = 1 \times 10^{-5}$. For these calculations, we used a constant value for $\kappa a = 0.5$.

Since for particles **B**, at a volume fraction of $\phi = 0.35$, we observed out-of-equilibrium phenomena that are not accounted for in the theory, such as stick-slip motion, we did not use this measurement in the calculation of the $\zeta$-potential and the particle charge. Also, we excluded the outlier (in the mobility data) for particles **A** at $\phi = 0.01$ from the analysis.

From the calculation, we obtain the full solution for the potential as a function of distance from the particle surface. Two examples are shown in Fig. 9 where the potential $\Psi(r)$ is drawn for two

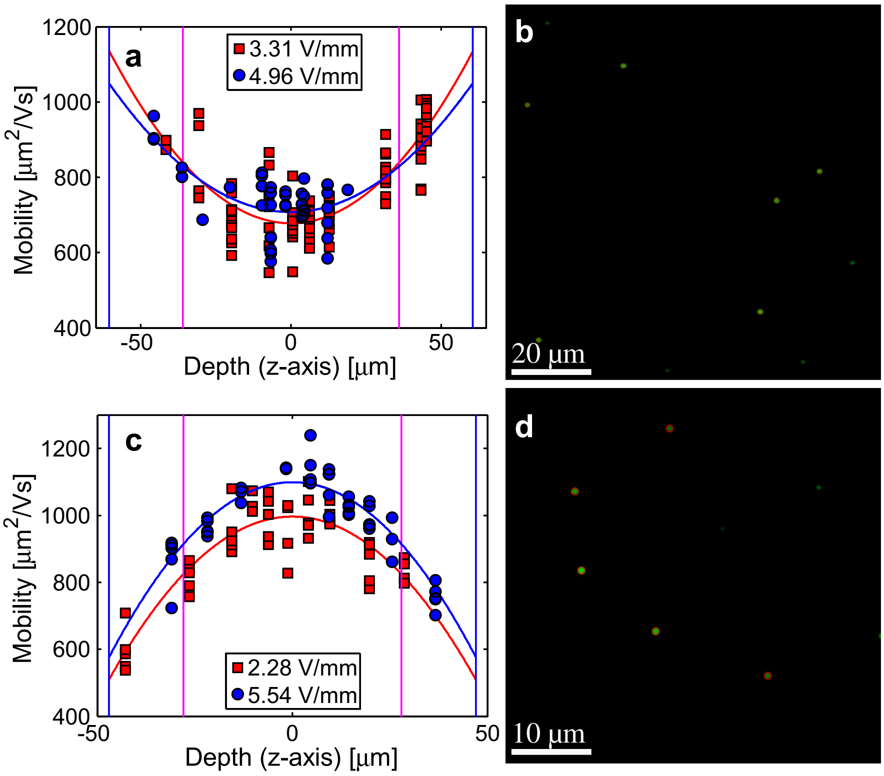

**Fig. 7.** Confocal images (taken in the $(xy)$-plane) and mobility profiles along the $z$-axis measured for (a and b) particles **A** at $\phi = 0.001$ for two different field strengths $E = 3.31$ V/mm (□) and $E = 4.96$ V/mm (○), and (c and d) particles **A** at $\phi = 0.0025$ at 2.28 V/mm (□) and 5.54 V/mm (○). Both the direction of the EOF and PF are inverted with increasing volume fraction. Blue vertical lines depict the upper and lower glass walls of the capillary. The magenta vertical lines denote the stationary planes. The red circles in the images mark particles recognized by the tracking algorithm. The center of the capillary is located at $z = 0$. (For interpretation of the references to color in this figure legend, the reader is referred to the web version of this article.)

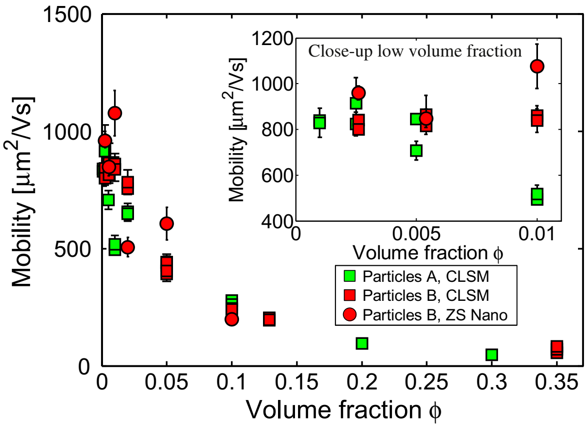

**Fig. 8.** The measured electrophoretic mobilities for particles **A** (green □) and **B** (red □) as a function of volume fraction. For particles **B**, also the mobilities measured by Doppler anemometry on the ZetaSizer Nano are shown (red ○). Inset: close-up of the electrophoretic mobilities measured at low volume fraction. (For interpretation of the references to color in this figure legend, the reader is referred to the web version of this article.)

neighboring particles in a dispersion with volume fraction $\phi = 0.0026$ (Fig. 9a) or $\phi = 0.1$ (Fig. 9b). Both calculations are performed for $\kappa a = 0.5$. The two green vertical lines denote the surfaces of the two neighboring particles. It can be observed that as the volume fraction increases, the double layers start to overlap. Note that the applied electric field $\mathcal{O}(1-10\,\mathrm{V/mm})$ is small compared to the electric field at the surface of the particles $|E| = \mathcal{O}(10-100\,\mathrm{V/mm})$.

In Fig. 10, the $\zeta$-potential is given for both particles **A** and **B** as a function of volume fraction $\phi$. The uncertainty in the screening parameter $\kappa a$ is marked by the lightly shaded area (blue). When $\kappa a$ is assumed to be constant (red circles), the $\zeta$-potential is roughly constant for different $\phi$. This corresponds to the idea that particles in chemical equilibrium with the solution maintain a constant potential. For comparison, we show the $\zeta$-potential that was obtained under the assumption of infinite dilution (green squares). Clearly, the correct treatment for particle interactions is important.

Alternatively, the potential with respect to the potential minimum at the boundary of the Kuwabara cell can be shown as a function of volume fraction (Fig. 11). As the volume fraction increases, the cell becomes smaller, and the potential at the boundary of the cell increases. As a result, $\zeta - \Psi(b)$ decreases and the potential landscape becomes more flat with respect to the dilute situation (see also Fig. 9).

From the calculated function for the potential $\Psi(r)$, we can obtain the electrokinetic particle charge using Gauss's theorem:

$$Q = -4\pi\epsilon_m\epsilon_0 a^2 \left[\frac{d\Psi}{dr}\right]_{r=a}, \qquad (12)$$

where $[d\Psi/dr]_{r=a}$ is the slope of the potential at the surface of the particle. In Fig. 12a and b, the calculated number of elementary charges $Z = Q/e$ is given as a function of volume fraction. Again, the calculation was performed for $\kappa = 0.5$ (blue points) and for $\kappa a = 0.3$ and $\kappa a = 0.7$.

The particle charge is reasonably constant at low volume fractions, but shows a decreasing trend with increasing volume fraction as the double layers start to overlap. For particles **B**, there seems to be first an increasing trend and a maximum at $\phi = 0.02$ (the same can be observed for the $\zeta$-potential). This trend is not

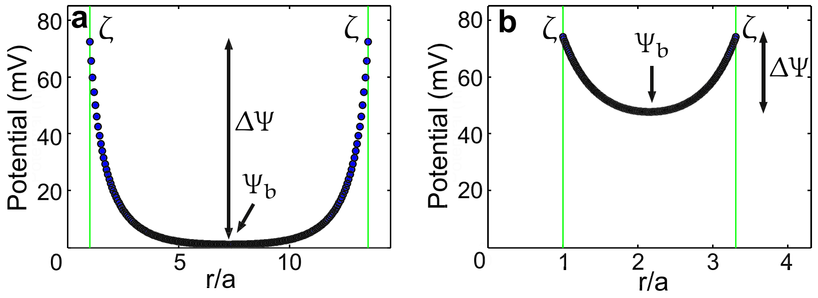

**Fig. 9.** The electric potential between the surfaces of two particles (vertical green lines) as a function of the distance $r$, given in units of the particle radius $a$. These data were calculated using [26] and our electrophoretic mobility data for particles **B** at (a) $\phi = 0.0026$ and $\kappa a = 0.5$ and (b) $\phi = 0.1$ and $\kappa a = 0.5$. It can be seen that for higher volume fractions, when the particles approach each other, the potential landscape flattens. (For interpretation of the references to color in this figure legend, the reader is referred to the web version of this article.)

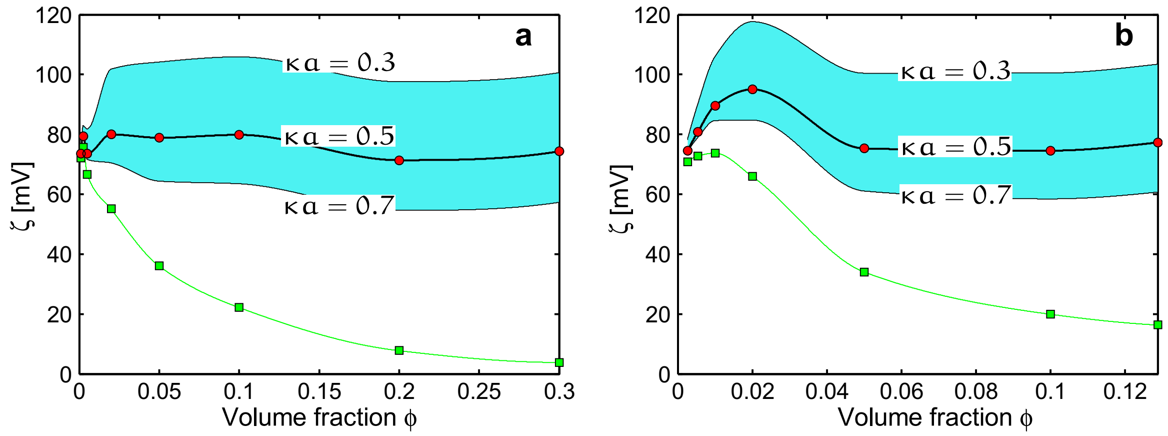

**Fig. 10.** The $\zeta$-potentials for (a) particles **A** and (b) particles **B** for different volume fractions calculated from the electrophoretic mobility. The red points (○) represent the calculations for a constant value of $\kappa a = 0.5$. The blue shaded area covers the results of the calculations for values of $\kappa a$ between 0.3 and 0.7. The green points (□) are the results assuming infinite dilution. The solid lines are guides to the eye. (For interpretation of the references to color in this figure legend, the reader is referred to the web version of this article.)

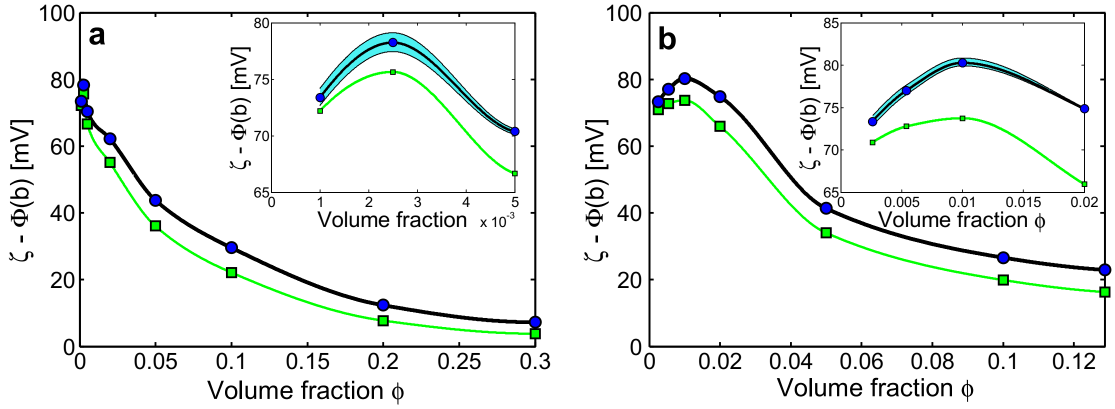

**Fig. 11.** The surface potential, given relative to the potential at the Kuwabara cell-boundaries $\zeta - \Psi(b)$ for (a) particles **A** and (b) particles **B** for different volume fractions calculated from the electrophoretic mobility. The red points (○) represent the calculations for a constant value of $\kappa a = 0.5$. The blue shaded area covers the results of the calculations for values of $\kappa a$ between 0.3 and 0.7. The green points (□) are the results assuming infinite dilution. The solid lines are guides to the eye. (For interpretation of the references to color in this figure legend, the reader is referred to the web version of this article.)

present for particles **A** and could therefore be coincidental. However, it could as well be related to a significant fraction of ions adsorbing to the wall (and consequently not to the surface of the particles) at low volume fractions, thus lowering the charge on the particles.

In addition, we display the predicted particle charges without the volume fraction correction (green squares in Fig. 12), again showing the importance of taking into account the effects of double-layer overlap. A lowering of the particle charge is expected if particles are to maintain a constant surface potential when they approach each other. We also note that, while the particle charge is low in comparison with colloids in an aqueous environment, the $\zeta$-potential is quite similar. This is in agreement with previous findings on dilute suspensions in apolar solvents [1]. Finally, we note

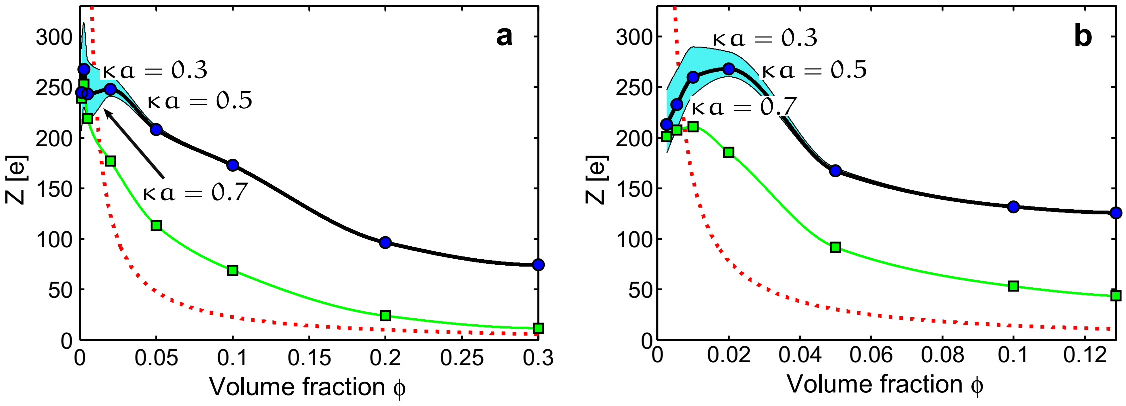

**Fig. 12.** Particle surface charge numbers $Z$ in elementary charges $e$ as a function of the volume fraction $\phi$ for (a) particles **A** and (b) particles **B** for different values of $\kappa a$. The blue shaded areas cover the results for different $\kappa a$. The red dotted line denotes the theoretical maximum charge that a single particle can acquire based on the ion concentration obtained by conductivity measurements of the pure solvent mixture (without colloids). The green points (□) show the result of the calculation without correcting for volume fraction effects. The solid lines are guides to the eye. (For interpretation of the references to color in this figure legend, the reader is referred to the web version of this article.)

that the decreasing charge with increasing $\phi$ was still observed when we repeated the calculations, using the same measured mobilities, but now assuming a much higher value of $\kappa a = 2$ (not shown). In this case, the $\zeta$-potential was seen to slightly decrease with increasing volume fraction.

Although the electrokinetics of our concentrated suspensions in apolar solvents is now clear, the origin of the charges is not. One possibility is that the particles adsorb some of the ions present in the solvent.

The dotted red line in Fig. 12a and b denotes the maximum number of elementary charges that a particle can acquire based on the amount of ions that were present initially in the pure solvent mixture:

$$Z_{\text{solvent}} = \frac{\rho_{\text{ion}}(\phi)}{\rho_{\text{col}}(\phi)} = \frac{\rho^0_{\text{ion}}(1-\phi)}{\rho_{\text{col}}(\phi)}, \tag{13}$$

where $\rho_{\text{ion}}$ and $\rho_{\text{col}}$ are the number densities of ions and colloids, respectively. The concentration inside the pure solvent mixture is measured to be (conductivity measurements) $\rho^0_{\text{ion}} \approx 4 \times 10^{15}\ \text{L}^{-1}$. As the volume fraction of colloids increased, the present ions had to be distributed over more colloids, reducing the number of charges per colloid. The fact that the measured charges were higher than the red line indicates that adsorption of ions which were present in the solvent before colloid addition cannot totally account for the particle charge. Apparently, part of the charge originated from the colloids themselves, either directly or indirectly.

Sterically stabilized PMMA particles (with a diameter of 2.16 μm) in CHB/cis-decalin were also used in earlier work by Royall et al. [15]. In their systems, different phases were obtained by increasing the colloidal volume fractions. At low volume fractions, their system was in a fluid phase; at intermediate volume fractions, the system crystallized (body centered cubic), a re-entrant fluid phase was found at slightly higher volume fractions and the system again crystallized at high volume fractions. For our particles ($\sigma_{\mathbf{A}} = 1.06$ μm and $\sigma_{\mathbf{B}} = 0.91$ μm, respectively), we observed a fluid phase at all probed volume fractions lower than or equal to $\phi = 0.3$.

Our results show that confocal microscopy offers a reliable and novel route to accurately measure the electrophoretic mobility in concentrated suspensions. In our case, i.e., the case of extended double layers, the mobility decreased nonlinearly with increasing volume fraction. This is an indication that the situation for thick overlapping double layers is more complicated than the simple linear dependence on volume fraction observed in studies for thin double layers [36,37,39]. Our calculations show that PMMA particles in a low-polar solvent decrease their surface charge as the volume fraction increases, while their $\zeta$-potential remains approximately constant. More research is required to study the mechanism of particle charging in more detail.

### 4.4. Self-diffusion in concentrated suspensions

From the two-dimensional trajectories of particles, we can not only obtain the electrophoretic mobility but also the self-diffusion coefficients in the directions parallel and perpendicular to the field axis. Here, particles are labeled with the index $i$, so that the position of particle $i$ can be written as $\mathbf{r}_i(t) = (r_i^{\parallel}(t), r_i^{\perp}(t))$, where we have split the position coordinate in a component parallel and another perpendicular to the field. Using these projected positions, we calculated the apparent self-diffusion coefficients both parallel $D(\Delta t)_{\parallel}$ and perpendicular $D(\Delta t)_{\perp}$ to the field:

$$D_\alpha(t,\Delta t) = \frac{\left\langle \left(\Delta r_i^\alpha(t,\Delta t) - \left\langle \Delta r_i^\alpha(t,\Delta t)\right\rangle\right)^2 \right\rangle}{(2\Delta t)}, \tag{14}$$

with

$$\Delta r_i^\alpha(t,\Delta t) = r_i^\alpha(t+\Delta t) - r_i^\alpha(t) \quad \forall \quad \alpha \in \{\parallel, \perp\}. \tag{15}$$

The angular brackets indicate averaging over all particles and all frames. Note that the mean-square displacements are calculated with respect to the average motion. That is to say, the average particle displacement is subtracted first, because it represents the drift velocity due to the electric field. For the fluctuations perpendicular to the field, $\left\langle \Delta r_i^\perp(t,\Delta t)\right\rangle = 0$. In this section, we express the diffusion in units of the diffusion at infinite dilution $D_0 = k_BT/(6\pi\eta a)$.

From the mean-square displacements parallel and perpendicular to the field axis, we observed that the fluctuations parallel and perpendicular to the field were almost the same. If there had been a high polydispersity in the electrophoretic mobility, it is expected that the spread in particle displacements would have been higher parallel to the field than perpendicular to the field. Since this is not the case, the polydispersity in the particle charges is likely to be low. This is different from observations in low-polar solvents where only a few elementary particles were present on each particle, giving rise to large variations in the electrophoretic mobility between different particles and even for the same particle in time [56].

For different depths $z$ in the capillary channel, $D(\Delta t)_{\parallel}/D_0$ and $D(\Delta t)_{\perp}/D_0$ were calculated for $\Delta t = 0.42$ s and are given for two

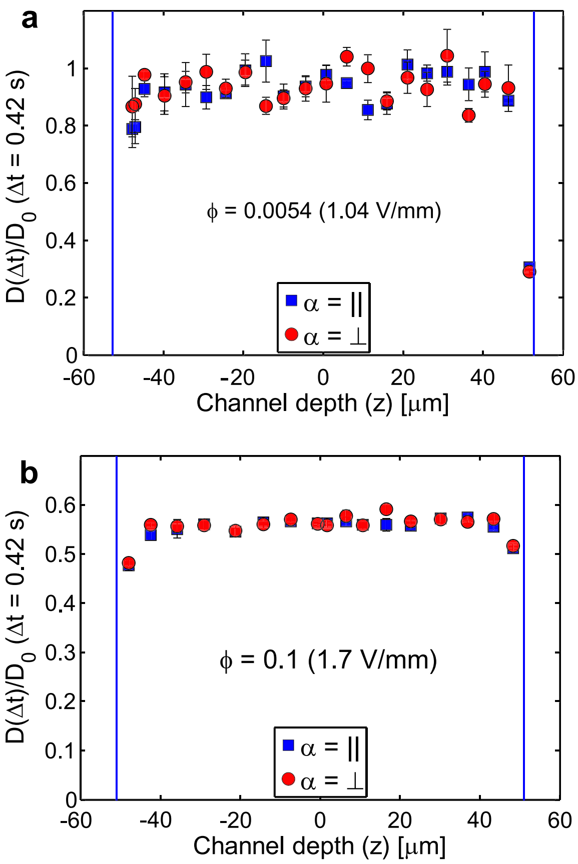

**Fig. 13.** Apparent self-diffusion coefficients $D(\Delta t)_{\parallel}$ and $D(\Delta t)_{\perp}$ expressed in units of the self-diffusion constant at infinite dilution, as a function of the channel depth $z$ for particles **B** at (a) $\phi = 0.0054$ (1.04 V/mm) and (b) $\phi = 0.1$ (1.71 V/mm) for different depths in the channel ($\Delta t = 0.42$ s). The (blue) vertical lines depict the positions of the lower and upper glass walls. The center of the capillary is located at $z = 0$. (For interpretation of the references to color in this figure legend, the reader is referred to the web version of this article.)

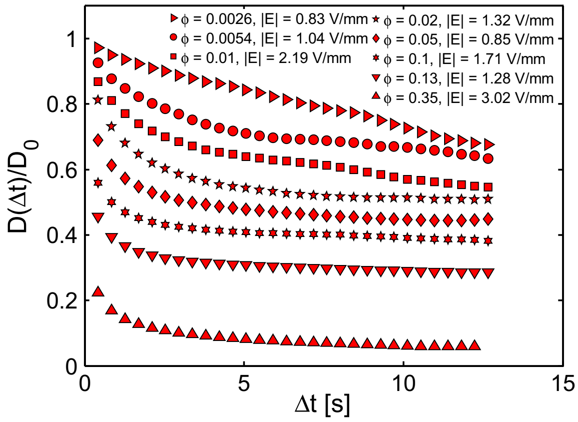

**Fig. 14.** The ratio between the apparent self-diffusion coefficient and the self-diffusion constant at infinite dilution $D(\Delta t)/D_0$ as a function of time for particles **B** and for different volume fractions. In all cases, a small electric field was present.

different volume fractions $\phi = 0.0054$ and $\phi = 0.1$ in Fig. 13. The self-diffusion coefficients are constant throughout the channel, showing that the EOF and PF did not affect the measurements. There was a small difference between the diffusion perpendicular and parallel to the field axis. Within approximately 3 μm of the glass walls, the diffusion of the particles was significantly lower than in the bulk (Fig. 13a, data point near the upper glass wall). This is caused by the fact that the hydrodynamic interactions are affected by the presence of the walls [57,58]. Moreover, we observed no significant dependence of the self-diffusion coefficients on the field strength for field strengths lower than 7 V/mm. Therefore, we expect the self-diffusion coefficients presented here to be almost identical to the case where no electric field was applied.

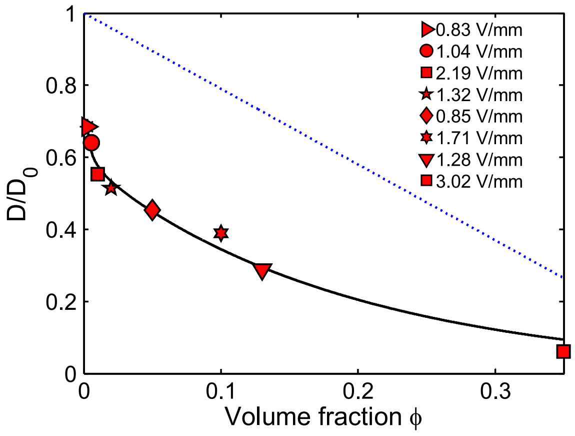

**Fig. 15.** Long-time self-diffusion coefficients $D$ in terms of $D_0$, obtained from Fig. 14 for particle species **B** as a function of the volume fraction $\phi$. In all cases, a small electric field was present. The black solid line is a guide to the eye. The blue dotted line shows the trend for hard spheres as given by $D_L = D_0(1 - 2.1\phi)$. (For interpretation of the references to color in this figure legend, the reader is referred to the web version of this article.)

Only in the case of the most concentrated dispersion ($\phi = 0.35$), layers on top of each other were observed to occasionally move in a stick-slip fashion [59]. Here, the character of the fluctuations becomes more complex than is the case for normal fluids moving in an electric field. Additional research is required to study the behavior of this dispersion, in an electric field and close to freezing, in more detail.

To study the effect of volume fraction, we averaged $D(\Delta t)_{\parallel}$ and $D(\Delta t)_{\perp}$ to obtain:

$$D(\Delta t) = \frac{D(\Delta t)_{\parallel} + 2D(\Delta t)_{\perp}}{3}, \tag{16}$$

as a function of time $\Delta t$ for different volume fractions. The time intervals for which we calculated the apparent self-diffusion coefficients are all on the time scales for which the colloids interact electrostatically with their neighbors $\Delta t > \tau_I$.

For all volume fractions, $D(\Delta t)$ decreases as the time interval $\Delta t$ between two measured particle positions increases and $D(\Delta t)$ asymptotically approaches a constant value which we take to be the long-time self-diffusion coefficient $D_L$. For the lower volume fractions ($\phi < 0.01$), where the mean-square displacements were calculated by averaging over a relatively small number of particles trajectories, the experimental error is higher than for the more concentrated suspensions. Generally, the measurement error in the mean-square displacements increased with $\Delta t$, since the number of trajectories decreases with the length of those trajectories (Fig. 5).

The long-time self-diffusion coefficients $D_L$ ($\Delta t \to \infty$) were estimated by taking the longest-time value from the curves in Fig. 14. The resulting long-time self-diffusion coefficients are given in Fig. 15. The dependence of $D_L$ on the volume fraction for hard spheres, interacting directly via hydrodynamic interactions as calculated by Batchelor and Cichocki and Felderhof [60,61], is also shown (dotted line). Even at low $\phi$, $D/D_0$ is well below unity, showing the importance of the interactions between the particles. This trend agrees with theoretical studies on the long-time self-diffusion for Yukawa particles [62,46–48], where a nonlinear decrease in the self-diffusion coefficient with volume fraction is seen as well.

Since the scanning speed of our confocal microscope is limited, we could not obtain values for the short-time self-diffusion constant. It would however be interesting to measure the short-time self-diffusion coefficient and compare the result with theoretically obtained values [63–65]. This can be achieved by using confocal microscopes that can operate at faster scanning speeds, or by using light scattering techniques.

## 5. Conclusions

We showed that by using a combination of confocal laser scanning microscopy, electrophoresis and particle tracking algorithms, we can accurately measure the electrophoretic mobility in concentrated suspensions of micron-sized colloidal particles. We applied this method to suspensions of charged PMMA-spheres in a low-polar solvent up to high volume fraction. Unlike in earlier studies that were performed in systems with higher electrostatic screening, we found that in our system the mobility decreases nonlinearly with increasing volume fraction $\phi$.

The screening length was estimated from the conductivity to be about $\kappa^{-1} \approx 1$ μm, so that $\kappa a \approx 0.5$. However, the conductivity depended on the particle concentration from volume fractions below about $\phi \approx 0.05$, after which it became roughly constant. The interpretation of the conductivity data is not straightforward, but it seems clear that part of the ions in the higher volume fraction dispersions originated from the particles and not from the solvent.

By using theory for electrophoresis that takes into account double-layer overlap, we have calculated the potential $\Psi(r)$ and the particle charge $Q = Ze$, where $Z$ is the number of elementary charges, from the electrophoretic mobility. We found that the $\zeta$-potential (at the surface of the particle) stays fairly constant around 80 mV, whereas the particle charge $Ze$ decreases nonlinearly from approximately $250e$ to less than $100e$ when $\phi$ increases from 0 to 0.3. When no correction for the volume was used, this decrease was even stronger. It has become clear that the majority of the particle charge must have originated as a result of the presence of the particles at all but the lowest volume fractions. We have also analyzed the diffusion of particles as function of volume fraction and observed a nonlinear decrease in the long-time self-diffusion coefficient which corresponds qualitatively well with earlier theoretical work.

## Acknowledgments

We would like to express our gratitude to Johan Stiefelhagen for particle synthesis and help with the assembly of the electric cells, Michiel Hermes, Mirjam Leunissen and Peter van Oostrum for fruitful discussions, and Frank Smallenburg and Joost de Graaf for the critical reading of this manuscript and for their useful comments (all Soft Condensed Matter, Utrecht University). Adam Wysocki (Institut für Festkörperforschung, Forschungszentrum Jülich) is thanked for kindly providing the Brownian dynamics computer simulation data that was used to test our tracking algorithm. We gratefully acknowledge NWO-CW for financial support.

## References

[1] P.H.C. van der Hoeven, J. Lyklema, Adv. Colloid Interface Sci. 42 (1992) 205–277.
[2] I.D. Morrison, Colloids Surf., A 71 (1993) 1–37.
[3] K. Klinkenberg, J.L. van der Minne, Electrostatics in the Petroleum Industry, New York, 1958.
[4] C.P. Royall, M.E. Leunissen, A. van Blaaderen, J. Phys.: Condens. Matter 15 (2003) S3581–S3596.
[5] A. Yethiraj, A. van Blaaderen, Nature 421 (2003) 513–517.
[6] G.H. Gelinck, H.E.A. Huitema, E. van Veenendaal, E. Cantatore, L. Schrijnemakers, J. van der Putten, T.C.T. Geuns, M. Beenhakkers, J.B. Giesbers, B.H. Huisman, E.J. Meijer, E.M. Benito, F.J. Touwslager, A.W. Marsman, B.J.E. Van Rens, D.M. De Leeuw, Nat. Mater. 3 (2004) 106–110.
[7] M.E. Leunissen, A. van Blaaderen, A.D. Hollingsworth, M.T. Sullivan, P.M. Chaikin, Proc. Natl. Acad. Sci. U.S.A. 104 (2007) 2585–2590.
[8] B.P. Binks, S.O. Lumsdon, Langmuir 16 (2000) 2539–2547.
[9] M.E. Leunissen, C.G. Christova, A.P. Hynninen, C.P. Royall, A.I. Campbell, A. Imhof, M. Dijkstra, R. van Roij, A. van Blaaderen, Nature 437 (2005) 235–240.
[10] T. Vissers, A. Wysocki, M. Rex, H. Löwen, C.P. Royall, A. Imhof, A. van Blaaderen, Soft Matter 7 (6) (2011) 2352–2356.
[11] T. Vissers, A. van Blaaderen, A. Imhof, Phys. Rev. Lett. 106 (2011) 228303.
[12] E.J.W. Verwey, J.T.G. Overbeek, Theory of the Stability of Lyophobic Colloids: The Interactions of Sol Particles Having an Electric Double Layer, New York, 1948.
[13] J.T.G. Overbeek, J. Colloid Interface Sci. 58 (1977) 408–422.
[14] W. Albers, J.T.G. Overbeek, J. Colloid Sci. 14 (1959) 501–509.
[15] C.P. Royall, M.E. Leunissen, A.-P. Hynninen, M. Dijkstra, A. van Blaaderen, J. Chem. Phys. 124 (2006) 244706.
[16] M.F. Hsu, E.R. Dufresne, D.A. Weitz, Langmuir 21 (2005) 4881–4887.
[17] D. Reinke, H. Stark, H.-H. v. Grunberg, A.B. Schofield, G. Maret, U. Gasser, Phys. Rev. Lett. 98 (2007) 038301.
[18] G.S. Roberts, T.A. Wood, W.J. Frith, P. Bartlett, J. Chem. Phys. 126 (2007) 194503.
[19] J.W. Merrill, S.K. Sainis, E.R. Dufresne, Phys. Rev. Lett. 103 (2009) 138301.
[20] M. Brunner, J. Dobnikar, H.H. von Grunberg, C. Bechinger, Phys. Rev. Lett. 92 (2004) 078301.
[21] A.V. Delgado, F. Gonzalez-Caballero, R.J. Hunter, L.K. Koopal, J. Lyklema, J. Colloid Interface Sci. 309 (2007) 194–224.
[22] R. Pelton, P. Miller, W. McPhee, S. Rajaram, Colloids Surf., A 80 (1993) 181–189.
[23] D.G. Yan, C. Yang, N.T. Nguyen, X.Y. Huang, Electrophoresis 27 (2006) 620–627.
[24] C. Yang, T. Dabros, D.Q. Li, J. Czarnecki, J.H. Masliyah, J. Colloid Interface Sci. 243 (2001) 128–135.
[25] J.D. Posner, Mech. Res. Commun. 36 (2009) 22–32.
[26] F. Carrique, F.J. Arroyo, A.V. Delgado, J. Colloid Interface Sci. 252 (2002) 126–137.
[27] D. Henry, Proc. Roy. Soc. Lond. A 133 (1931) 106.
[28] H. Ohshima, J. Colloid Interface Sci. 168 (1994) 269.
[29] A. Loeb, P. Wiersema, J. Overbeek, The Electrical Double Layer around a Spherical Particle, MIT Press, Cambridge, Mass, 1961.
[30] J.T.G. Overbeek, Kolloid Beihefte 54 (1943) 287.
[31] F. Booth, Proc. Roy. Soc. Lond. A 203 (1950) 514.
[32] P. Wiersema, A. Loeb, J.G. Overbeek, J. Colloid Interface Sci. 22 (1964) 78.
[33] R. O'Brien, L. White, J. Chem. Soc. Faraday II 74 (1978) 1607.
[34] R. Hunter, Zeta Potential in Colloid Science, London, 1981.
[35] D. Long, A. Ajdari, Eur. Phys. J. E 4 (2001) 29–32.
[36] J.L. Anderson, J. Colloid Interface Sci. 82 (1981) 248–250.
[37] C.F. Zukoski, D.A. Saville, J. Colloid Interface Sci. 115 (1987) 422–436.
[38] A.T. Perez, E. Lemaire, J. Colloid Interface Sci. 279 (2004) 259–265.
[39] M. Medrano, A.T. Perez, L. Lobry, F. Peters, Langmuir 25 (2009) 12034–12039.
[40] V. Lobaskin, B. Dunweg, M. Medebach, T. Palberg, C. Holm, Phys. Rev. Lett. 98 (2007) 176105.
[41] S. Levine, G. Neale, J. Colloid Interface Sci. 47 (1974) 520.
[42] S. Kuwabara, J. Phys. Soc. Jpn. 14 (1959) 527.
[43] H. Ohshima, J. Colloid Interface Sci. 188 (1997) 481–485.
[44] J.P. Hsu, E. Lee, F.Y. Yen, J. Chem. Phys. 112 (2000) 6404–6410.
[45] F. Carrique, F.J. Arroyo, M.L. Jimenez, A.V. Delgado, J. Phys. Chem. B 107 (2003) 3199–3206.
[46] H. Löwen, G. Szamel, J. Phys.: Condens. Matter 5 (1993) 2295–2306.
[47] G. Nagele, M. Kollmann, P. Raphael, A.J. Banchio, Mol. Phys. 100 (2002) 2921–2933.
[48] G. Nägele, P. Baur, Europhys. Lett. 38 (1997) 557.
[49] G. Bosma, C. Pathmamanoharan, E.H.A. de Hoog, W.K. Kegel, A. van Blaaderen, H.N.W. Lekkerkerker, J. Colloid Interface Sci. 245 (2002) 292–300.
[50] J.C. Crocker, D.G. Grier, J. Colloid Interface Sci. 179 (1996) 298–310.
[51] R. Besseling, L. Isa, E.R. Weeks, W.C.K. Poon, Adv. Colloid Interface Sci. 146 (2009) 1–17.
[52] L. Drain, The Laser Doppler Technique, John Wiley Press, USA, 1980.
[53] F. Durst, A. Melling, J. Whitelaw, Principles and Practice of Laser Doppler Anemometry, Academic Press, London, 1976.
[54] M. Campisi, D. Accoto, P. Dario, J. Chem. Phys. 123 (2005) 204724.
[55] S. Ahualli, A.V. Delgado, C. Grosse, J. Colloid Interface Sci. 301 (2006) 660–667.
[56] F. Strubbe, F. Beunis, K. Neyts, Phys. Rev. Lett. 100 (2008) 218301.
[57] J. Happel, H. Brenner, Low Reynolds Number Hydrodynamics, Martinus Nijhoff Publishers, The Hague, 1991.
[58] T.M. Squires, M.P. Brenner, Phys. Rev. Lett. 85 (2000) 4976–4979.
[59] H. Yoshizawa, J. Israelachvili, J. Phys. Chem. 97 (1993) 11300–11313.
[60] G.K. Batchelor, J. Fluid Mech. 131 (1983) 155–175.
[61] B. Cichocki, B.U. Felderhof, J. Chem. Phys. 89 (1988) 3705–3709.
[62] J. Wagner, W. Hartl, H. Walderhaug, J. Chem. Phys. 114 (2001) 975–983.
[63] D.N. Petsev, N.D. Denkov, J. Colloid Interface Sci. 149 (1992) 329–344.
[64] G.A. Schumacher, T.G.M. van de Ven, Faraday Discuss. 83 (1987). 75–+.
[65] M. Watzlawek, G. Nägele, Phys. Rev. E 56 (1997) 1258.